Polarization filtering induced by imaging systems: Effect on image structure

T. Grosjean and D. Courjon*

Laboratoire d'Optique P. M. Duffieux, UMR 6603, CNRS/Université de Franche-Comté, IMFC FR67,
UFR Sciences et Techniques, 25030 Besançon cedex, France

In this paper are reported the results concerning the experimental study of the interaction between the vectorial amplitude of an optical field and imaging systems. It is shown that far-field as well as near-field imaging systems beside their spatial frequency filtering ability, also act as polarization filters playing a determinant role on the image structure. This conclusion is drawn from an experimental and theoretical study involving a radially polarized Bessel beam used as a test object.

I. INTRODUCTION

The principle of imaging is generally defined as the result of spatial frequency filtering due to limited optical aperture of optical systems [1]. Theories leading to this conclusion are derived from Abbe interference-based approach as well as Rayleigh diffraction analysis [2]. Unfortunately, most of the developed models do not take into account the polarization state of the light. The reason is probably both the complexity of the physical problem and the use of natural unpolarized light in most cases. However, thanks to progress in near-field microscopy, several powerful models have been carried out allowing a better knowledge of light-matter interaction in the near zone [3,4].

These models have pointed out the role of polarization in near-field images and have suggested that the field diffracted by a sample is strongly polarization dependent [5,6]. These conclusions have been often verified experimentally [7,8]. However, the understanding of the interaction between the imaging system (objective or near-field probes) and the vectorial amplitude of the field diffracted by the sample has only been the field of research of very few theoretical works [9,10] and no experimental investigations have been proposed. This can be explained by the difficulty to find a test object enabling the study of the phenomenon.

In this paper, we present our first experimental results concerning the imaging of propagating nonparaxial Bessel beams which are simply generated from an annular-shaped focused beam radially polarized. The use of such particular field distributions as test object allows us to experimentally estimate the effect of polarization on image formation and more particularly to study the polarization filtering of both classical imaging systems (refractive optics) and near-field imaging systems (scanning dielectric tips).

II. PRINCIPLE

A. The test object

The optical system allowing the creation of the test object is composed of a high numerical aperture (NA) objective coupled with an annular mask of diameter d and thickness e located in the objective rear pupil plane (see Figs. 1 and 2). The technique has been first performed in the paraxial case in which the high NA objective is replaced by a lens with a long focal length [11]. The angular spectrum of the transmitted nondiffracting field is given by the transmittance of the annular mask. The diameter d defines the size of the Bessel beam, whereas e is responsible for its spectral distribution; it is chosen as narrow as possible. The objective is represented by its principal planes H and H' (see Ref. [12]).

The use of a radially polarized incident beam leads to a very simple analytical expression for the Bessel beam allowing the direct observation of the polarization filtering phenomenon. The nondiffracting field then takes the simple form [13]:

$$E_x(r,\xi) \propto -i\cos(\theta)\cos(\xi)J_1(\alpha r), \qquad (1)$$

$$E_y(r,\xi) \propto -i\cos(\theta)\sin(\xi)J_1(\alpha r), \qquad (2)$$

$$E_z(r,\xi) \propto \sin(\theta)J_0(\alpha r), \qquad (3)$$

where (r,ξ) are the position polar coordinates. α, θ are constants. Functions J_m are Bessel functions of first kind and m order. Let us call $I_z = |E_z|^2$, $I_r = |E_x|^2 + |E_y|^2$, and the intensity $I = I_r + I_z$. From Eqs. (1) and (2) it appears that I_r is proportional to J_1^2 and from Eq. (3) that I_z is proportional to J_0^2. We note that J_1^2 is almost the complementary function of J_0^2 since its maxima correspond approximately to the zeros of J_0^2 and reciprocally. Therefore, by comparing the experimental images with the computed intensity I, the effect of the weight of the component E_z versus $E_x + E_y$ is straightforward. The radially polarized Bessel beam is then a valuable test object to study the E_z component filtering by imaging systems.

B. The polarization filtering process

The so created Bessel beam is then explored either by mean of an objective (Fig. 1) or by a near-field microscope dielectric tip (Fig. 2). The gray-level images show the computed intensity distribution in the object and image planes in the two considered cases (far field and near field).

In the far-field case (Fig. 1), the "optical lever" created by the unbalanced distances p and p' implies $\theta' \ll \theta$ which is

*Electronic address: thierry.grosjean@univ-fcomte.fr
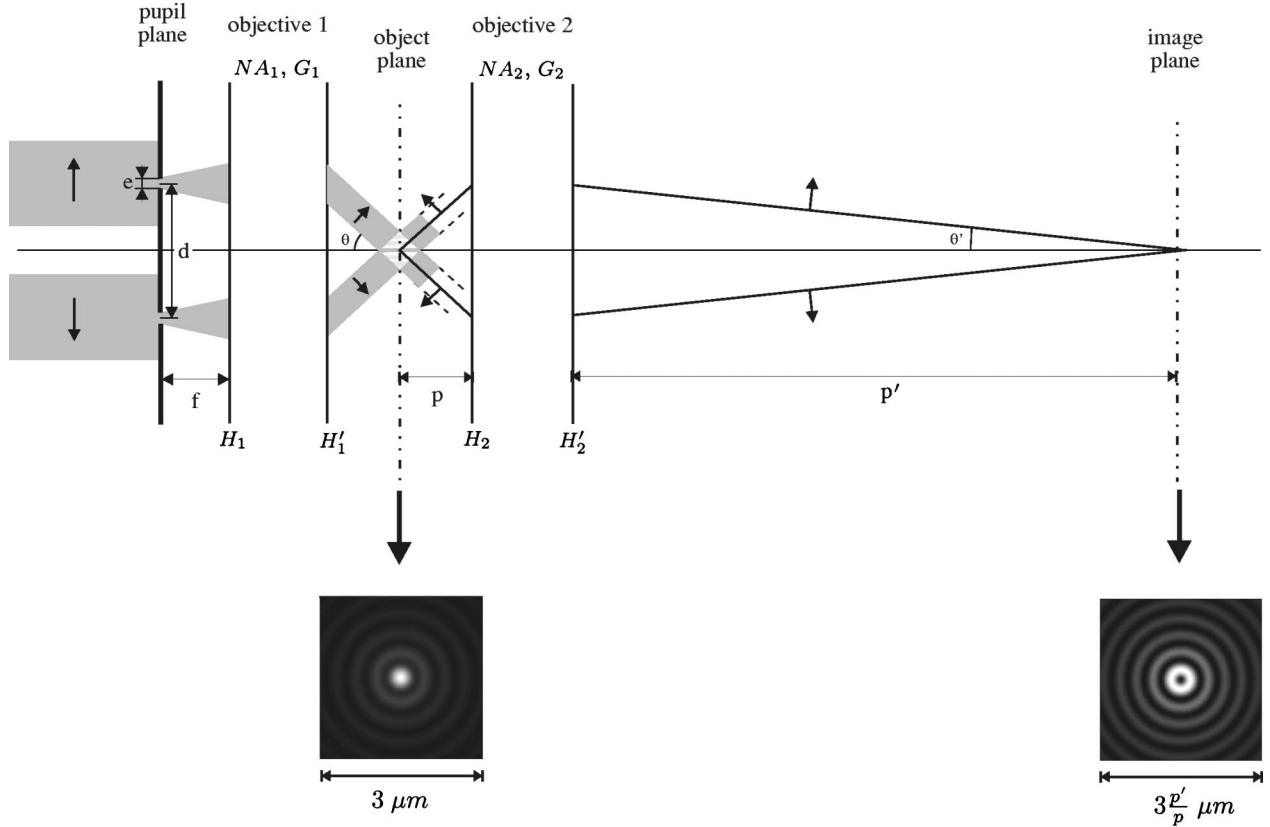
FIG. 1. Setup involving a microscope objective as magnifying far-field imaging system. Objective 1 generates the test object which is imaged by objective 2. $NA_1 = NA_2 = 0.85$, magnification $G_1 = G_2 = 63$. H_1, H_1' and H_2, H_2' are the principal planes of objectives 1 and 2, respectively.

responsible for the attenuation of the E_z component in the image field distribution. Since the E_z component generates the J_0 Bessel function [Eq. (3)], the resulting image field distribution reduces approximately to I_r, that is to J_1^2. The J_1 function is predominant in the image as shown in Fig. 1. The consequence is a widening of the image of the field waist leading to a significant loss of confinement.

In the near-field imaging case (Fig. 2), light diffracted by the apex is collected in a cone materialized by the tip itself. The polarization filtering behavior of such a tip and the effect on image structure have been simulated in Ref. [9]. In that work, the apex is modeled as a small electric dipole scattering the field (E_x, E_y, E_z) diffracted by a sample into a solid angle defined by the angle δ. Since light is guided to the detector through an optical fiber, δ is limited either by the aperture of the taper or by the cutoff parameters of the fiber.

The detected intensity can be then written as

$$I_d(x,y,z) \propto (|E_x|^2 + |E_y|^2)K_{xy} + |E_z|^2 K_z, \qquad (4)$$

with $K_{xy} = 16 - 15\cos\delta - \cos 3\delta$ and $K_z = 16 - 18\cos\delta + 2\cos 3\delta$.

Although the polarizability of the electric dipole is assumed to be isotropic, Fig. 3 shows that the three compo-

nents of the field diffracted by a sample cannot be transferred with the same weight in the image structure when $\delta \neq \pi/2$.

Moreover, it appears for the smallest values of δ, that the E_z components of the diffracted field distribution can be almost totally filtered in the image structure. It is precisely the case in our configuration for which δ is limited to values smaller than 1° by the cutoff parameters of the monomode fiber used to create the tip. As shown in Fig. 2, E_z is strongly attenuated in the image structure. The J_0^2-like distribution of I in the object plane is transformed in a J_1^2-like distribution in the image structure.

III. EXPERIMENTS

The nonparaxial Bessel beams are created with a ($\times 63$, NA = 0.85) objective. The width of the annular transmittance e has been set to 50 μm. This value is a good compromise between the diffraction effect of the annular screen and the quantity of transmitted energy. For such a width, the divergence of the experimentally measured focused beam does not exceed 5° (with the objective we have used). Therefore, the differences between the obtained focused field distribution and the perfect nonparaxial Bessel beam can be neglected as shown in Fig. 4. This figure displays a simulation of the difference (in absolute value) be-
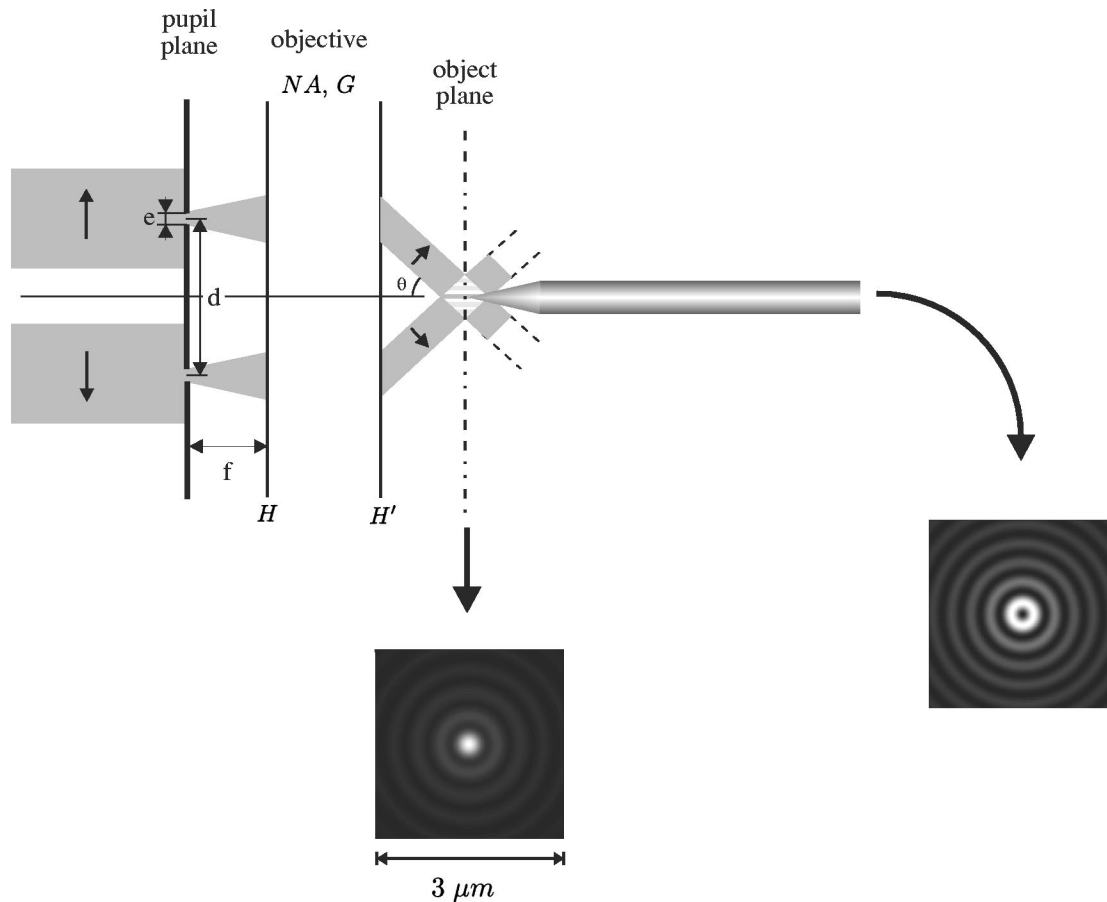
FIG. 2. Setup involving a tapered fiber tip as the collecting near-field probe.

tween the intensity distribution of the focused beam, in the objective focal plane, and the intensity distribution of the Bessel beam. The difference is expressed in normalized units. In this example $\theta = 40°$ for the Bessel beam, whereas $37.5° < \theta < 42.5°$ for the focused beam. The calculations are based on Ref. [14] for the focused beam and on Ref. [13] for the Bessel beam.

Unfortunately, it is generally admitted that the radial polarization state is not easy to obtain without carrying out more or less complex interference-based devices. However, we have recently proposed a different and robust technique solving this tricky problem which uses the filtering properties of two segments of slightly mismatched fibers [15].

In the far-field case, the objective used as an imaging system has the same characteristics as that of the Bessel beam generator objective [Fig. 5(a)]. The two objectives are
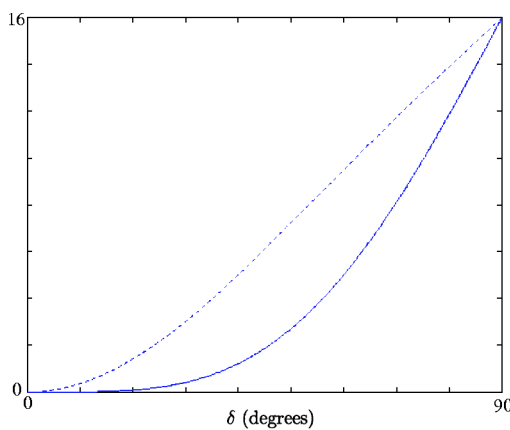
FIG. 3. Plot of coefficients K_{xy} (dashed curve) and K_z (solid curve) versus δ.
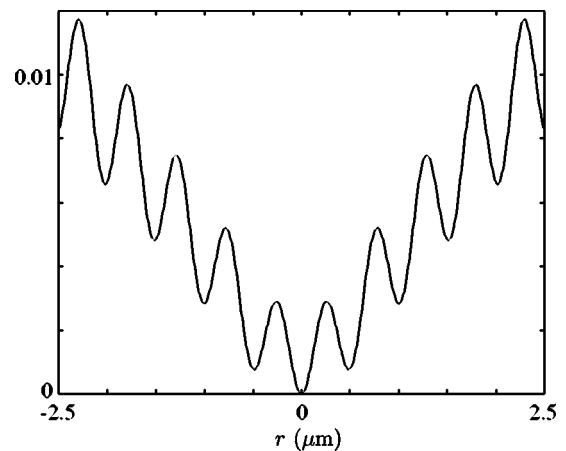
FIG. 4. Difference between the intensity distributions of a Bessel beam ($\theta = 40°$) and the focused beam in the focal plane of the objective (normalized unit). In the latter case, the beam divergence is defined as $37.5° < \theta < 42.5°$.

(a)

(b)
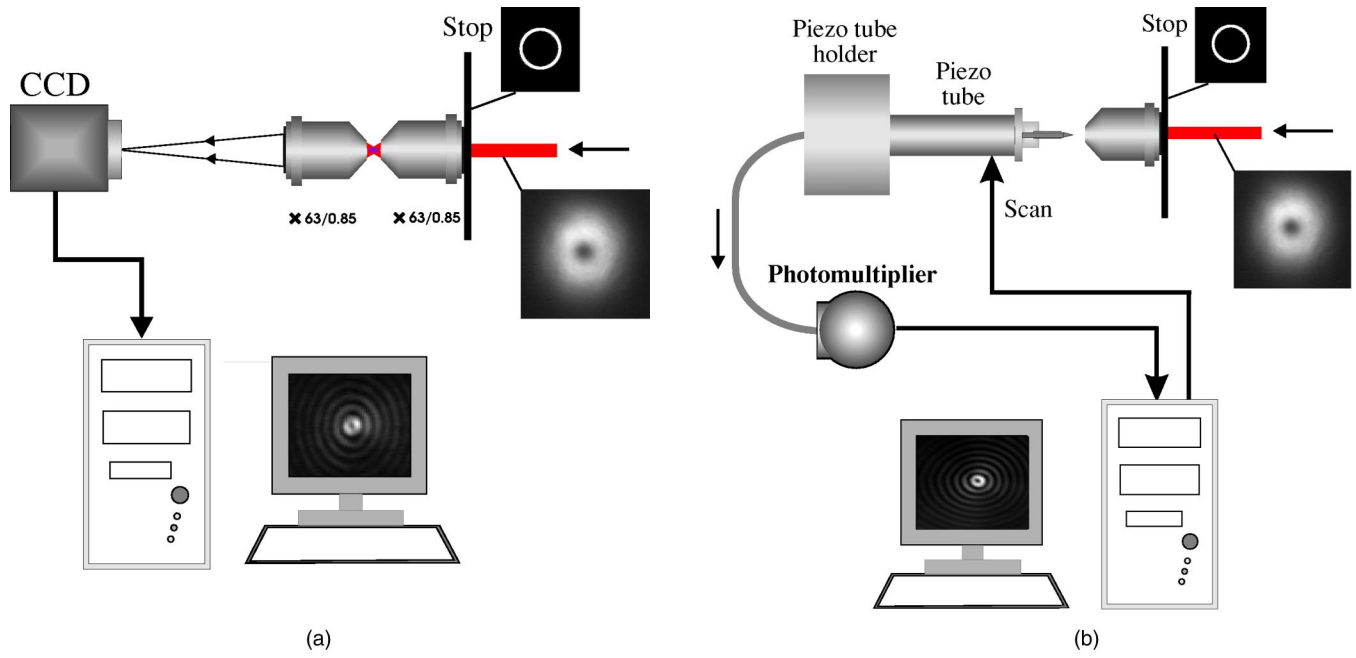
FIG. 5. Experimental setup in the far-field case (a) and in the near-field case (b).

(a)

(b)

(c)

(d)
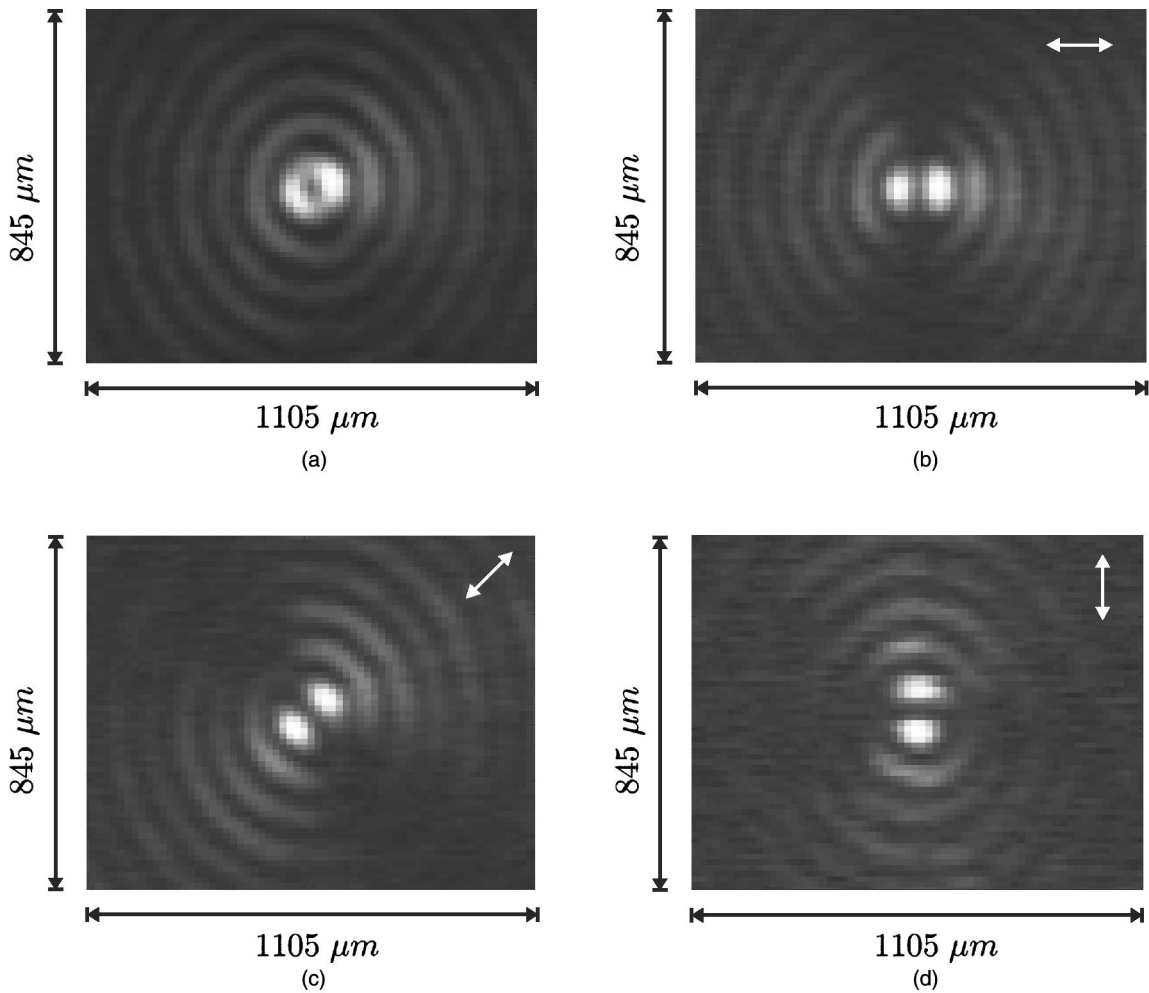
FIG. 6. Experimental light distribution in the image plane of microscope objective 2 ($\times$63,NA$=$0.85). (a) Direct image, [(b), (c), (d)] image when the incident beam passes through a polarizer whose axis is oriented along the indicated arrows.
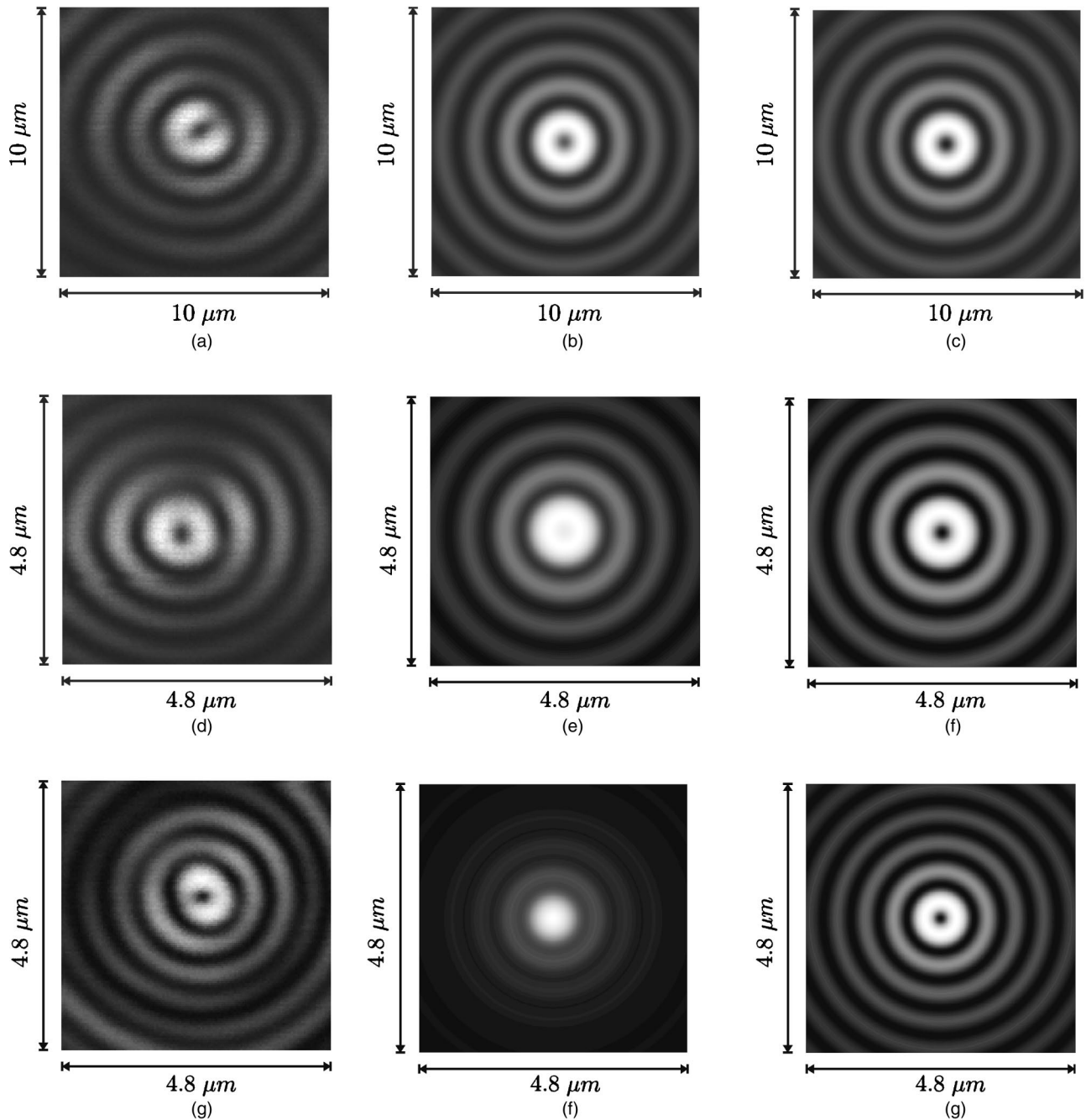
FIG. 7. Comparison between experimental images [(a), (d), (g)] obtained by near-field scanning by means of a bare tapered fiber tip and simulations of the intensities in the tip apex plane [(b), (e), (h)] and the detected intensities [(c), (f), (i)]. Three aperture angles for the Bessel beams are considered: $\theta=15°$ [(a), (b), (c)], $\theta=30°$ [(d), (e), (f)], and $\theta=40°$ [(g), (h), (i)].

precisely set parallel to the incident beam axis by means of two separate $XYZ\theta$ differential-screw stages. A charged-coupled device camera is set in the image plane and gives the experimental images.

The detection stage proposed in Fig. 5(b) is usual in local probe microscopy. It is composed of two positioning stages, the first one, combines a XY-differential-screw stage and a Z-piezo actuator allows the rough XYZ displacement of the tip, whereas the second one, composed of a segmented piezo tube allows the fine XYZ scanning of the Bessel beam. The

bare tip is made by heating and pulling a monomode optical fiber (at $\lambda=632.8$ nm) but other ways are possible. It works in collection mode and no distance control feedback is used. The scanning is performed in the region of existence of the Bessel beam, near the object focal plane of the objective.

IV. RESULTS

Figure 6 shows the experimental image (a) and three linearly polarized images (a polarizer is set before the pupil

stop) obtained in the far-field case. The direction of the polarizer axis is indicated by arrows on the figures. These results confirm that polarization perturbations induced by diffraction through the annular slit are negligible.

For the near-field experiments, three different angles θ for the Bessel beam have been tested by changing the diameter of the annular stop. For each angle ($15°,30°,40°$), both intensity distribution in the tip apex plane and intensity detected by the tip have been computed. The theoretical and experimental results are reported in Fig. 7. We note that, whatever the angle between $15°$ and $40°$, the detected intensity is proportional to a J_1^2-like function, whereas the computed intensity in the apex plane varies from J_1^2-like to J_0^2-like distributions versus the angle. These results confirm that the aperture of the tip is a strongly limiting factor. Despite our efforts, no confined field has been observed.

V. DISCUSSION

Although Bessel beams are used as test object because of their well-known structure, our conclusions can be generalized since the E_z component is always more or less suppressed in the image structure whatever the object complexity.

Therefore, independently of the classical notion of frequency filtering, far-field imaging systems provide magnified images which are always different from object field distributions. In fact, the filtering process is significant only in the case of high magnifying factors. For small magnifying factors this filtering effect can be neglected. It is worth noting that the $×1$ imaging system preserve the longitudinal component.

In the near-field case, the situation is similar since it has been shown both theoretically and experimentally that the tip aperture plays the role of a filter for the E_z component. This effect has to be taken into account when near-field images are interpreted. The effect of E_z filtering process can, however, be limited by choosing high aperture tips. In that case, the use of an optical tapered fiber becomes questionable. Moreover, the use of apertureless detection type (Ref. [16]) should allow the transfer of the three field components. Finally, the positioning of a single fluorescent molecule on the apex of the tip could lead the novel probe to transfer only the component parallel to the dipole moment of the molecule. This polarization filtering behavior can be observed, for example, in Ref. [17].

VI. CONCLUSION

Radially polarized propagating nonparaxial Bessel beams have been used to test far-field and near-field imaging systems. Due to simple analytical expression for the field distribution, it has been shown both theoretically and experimentally that the E_z component of the field diffracted by a sample is strongly attenuated in the image structure. Therefore, spatial frequency attenuation due to the limited aperture of imaging systems is not the only factor modifying the light distribution in the image, polarization filtering plays a significant role on the image formation. For high numerical aperture microscopes this phenomenon, which is generally neglected, must be taken into account definitely. Holding for any imaging system, the family of confocal microscopes could clearly gain by such an approach of the resolution problem.

[1] M. Born and E. Wolf, *Principle of Optics* (Pergamon, New York, 1959), Chap. 9, pp. 479–489.

[2] M. Born and E. Wolf, *Principle of Optics* (Pergamon, New York, 1959), Chap. 8, pp. 413–423.

[3] D.V. Labeke and D. Barchiesi, J. Opt. Soc. Am. A **9**, 732 (1992).

[4] C. Girard, A. Dereux, and O. Martin, Phys. Rev. B **49**, 13 872 (1994).

[5] C. Girard, A. Dereux, O. Martin, and M. Devel, Phys. Rev. B **52**, 2889 (1995).

[6] H. Furukawa and S. Kawata, Opt. Commun. **196**, 93 (2001).

[7] J. Weeber, E. Bourillot, A. Dereux, J. Goudonnet, Y. Chen, and C. Girard, Phys. Rev. Lett. **77**, 5332 (1996).

[8] D. Courjon, C. Bainier, and M. Spajer, J. Vac. Sci. Technol. B **10**, 2436 (1992).

[9] D. Barchiesi and D. Van Labeke, in *Near Field Optics*, Vol. 242 of *NATO Advanced Studies Institute, Series E Applied Sciences*, edited by D.W. Pohl and D. Courjon (Kluwer Academic Publishers, Dordrecht, 1993), pp. 179–188.

[10] C. Girard and X. Bouju, J. Opt. Soc. Am. B **9**, 298 (1992).

[11] J. Durnin, J. Miceli, and J. Eberly, Phys. Rev. Lett. **58**, 1499 (1987).

[12] M. Pluta, *Advanced Light Microscopy Vol. 1: Principles and Basic Properties* (Elsevier, New York 1988), Chap. 2, p. 183.

[13] T. Grosjean and D. Courjon, J. Microsc. **202**, 273 (2000).

[14] B. Richards and E. Wolf, Proc. R. Soc. London, Ser. A **253**, 358 (1959).

[15] T. Grosjean, D. Courjon, and M. Spajer, Opt. Commun. **203**, 1 (2002).

[16] P. Adam, P. Royer, R. Laddada, and J.L. Bigeon, Appl. Opt. **37**, 1814 (1998).

[17] L. Novotny, M. Beversluis, K. Youngworth, and T. Brown, Phys. Rev. Lett. **86**, 5251 (2001).